Morphological Analysis of Brownian Motion for Physical Measurements

Élodie Puybareau[1,2], Hugues Talbot[2], Noha Gaber[3], and Tarik Bourouina[2]

[1] EPITA Research and Development, 14-16 rue Voltaire, F-94276 Le Kremlin-Bicetre
[2] Université Paris-Est / ESIEE, 2 Boulevard Blaise-Pascal, F-93162 Noisy-le-Grand
[3] National Oceanic and Atmospheric Administration, Washington, D.C., USA

Abstract. Brownian motion is a well-known, apparently chaotic motion affecting microscopic objects in fluid media. The mathematical and physical basis of Brownian motion have been well studied but not often exploited. In this article we propose a particle tracking methodology based on mathematical morphology, suitable for Brownian motion analysis, which can provide difficult physical measurements such as the local temperature and viscosity. We illustrate our methodology on simulation and real data, showing that interesting phenomena and good precision can be achieved.

Keywords: Random walk, particle suspension, particle tracking, segmentation.

1 Introduction

Brownian motion was first described by Robert Brown in 1828 [1]. He observed the jittery motion of microscopic particles suspended in water, but could not explain it at the time. Einstein, in one of his 1905 *annus mirabilis* articles [2] was able to propose a consistent theory of Brownian motion based on random walks. He explained that the observed motion was the result of random collisions between water molecules and the observed particles. Due to the discrete nature of these collisions, at any point in time the forces acting on a particle are constantly changing, resulting in an unpredictable trajectory. Jean Perrin carefully designed experiments that proved that the Einstein theory was correct, the first convincing observational evidence of the existence of molecules [3]. The Einstein theory together with the Perrin experiements allowed estimations of the size of atoms and how many atoms there are in a mole (the Avogadro number). This earned Jean Perrin the Nobel prize in physics in 1926.

Einstein had sought to estimate the distance a Brownian particle travels in a given time. Because the number of collisions between molecules and particles is enormous, classical mechanics could not be used. Instead Einstein called upon the notion of random walks. Using the ensemble motion of a large number of particles, Einstein was able to show that the density of particles obeys a diffusion equation.

Random walks are an interesting and ubiquitous model for a number of stochastic processes. Besides physics, they are useful in finance [4], ecology [5], biology [6], chemistry [7], and of course imaging [8]. They form the basis of stochastic optimisation, particularly MCMC methods [9,10]. In imaging, these approaches led to Markov Random Fields methods [11].

Random walk also allow the construction of complex models [12], both unpredictable at the short timescale and highly regular in the long run. Indeed, many stochastic processes converge to the Brownian motion model, which is one of the simplest yet most irregular stochastic evolution process.

Random walks have been very widely studied. In this article, we are not so much interested in their phenomena per se, as we are in the image analysis of Brownian motion. Indeed, we show that the image analysis of Brownian motion can lead to useful physical measurements. As far as we know, Brownian motion has been used to estimate temperature before [13] but not through automated image analysis methods.

In the remainder of this article, we define the Brownian motion model and its more precise links to random walks and diffusion phenomena in section 2. We describe our sequence processing pipeline in 3. We then formalize the expected results of physical Brownian motion via particle tracking in section 4. Finally we show results on simulations and actual data.

2 Brownian motion, random walks and diffusion

What is now widely referred to as "Brownian motion" is no longer the physical phenomenon that Robert Brown observed in 1828. Instead, it is a process model, also called the Wiener process.

Definition 1. *Let W_t be a random process with the following properties:*

1. *$W_0 = 0$ a.s ;*
2. *W has independent increments, meaning if $0 \leq s_1 < t_1 \leq s_2 < t_2$ then $W_{t_1} - W_{s_1}$ and $W_{t_2} - W_{s_2}$ are independent random variables;*
3. *W has Gaussian increment, meaning $W_{t+u} - W_t \sim \mathcal{N}(0, u)$, i.e. $W_{t+u} - W_t$ is Normally distributed with variance u;*
4. *W is continuous a.s.*

This process is non-smooth at all scale (no matter how small $t_1 - s_1$ is), and so largely theoretical, but can be well approximated by random walks.

Definition 2. *Let $\xi_1, \xi_2, \ldots$ be i.i.d random variables with mean 0 and variance 1, Let W_t^r be the following random step function:*

$$W_n^r(t) = \frac{1}{\sqrt{n}} \sum_{1 \leq k \leq \lfloor nt \rfloor} \xi_k$$

This function is called a random walk. We now have the following theorem:

Theorem 1. *As $n \to \infty$, $W_n^r(t)$ converges to the Wiener process W_t.*

Proof. The proof is given in [14], but the idea is intuitive. Indeed, $W_n^r(0) = 0$; moreover, since the ξ_i are independent, $W_n^r(t)$ has independent increments; for large n, $W_n^r(t) - W_n^r(s)$ is close to $\mathcal{N}(0, t-s)$ by the central limit theorem (CLT). The continuity argument is more difficult. Since W_n^r is a step function, it is continuous a.e, but this is of little utility in the limit. However as $n \to +\infty$, the jumps tend to zero even though jumps may be arbitrary large initially. This guarantees the almost sure continuity.

In practical terms, this means that a sum of i.i.d Normal random variables converges to the Brownian motion process, and so is easy to simulate. In fact, because so many distributions converge to the Normal distribution by the CLT, we can use simpler distributions for the steps. For instance, binary steps where $\xi_i \in \{+1/-1\}$ with equal probabilities instead of Normal steps are fairly standard.

This process extends to any dimension by choosing vector steps with i.i.d. components (binary or Normal). In the binary case, this corresponds to random walks on an infinite regular grid. There are a number of interesting facts regarding random walks and Brownian motion, in particular:

$$E[W_t] = 0 \tag{1}$$
$$V[W_t] = t \tag{2}$$

A proof in the discrete case is given below. Pólya showed [15] that random walks return to the origin with probability 1 in 1-D and 2-D but not for dimensions greater than 2.

2.1 Average and variance of the position

In the simplest case, we consider a random walker making steps of length l in one dimension. This means that at each timestep s_i of duration τ, this random walker can move one position to the right or left with equal probability.

$$s_i = \begin{cases} -l \text{ with probability } 1/2 \\ +l \text{ with probability } 1/2 \end{cases} \tag{3}$$

After N steps (at time $N\tau$), the position of the walker is

$$x(N) = \sum_{i=1}^{N} s_i. \tag{4}$$

with going left or right equiprobable. Starting from 0, the average position is

$$E[x(N)] = 0 \tag{5}$$

I.e. the average position is always at the origin. However the variance of the position changes with time. We write

$$x^2(N) = \left(\sum_{i=1}^{N} s_i\right)^2 = \sum_{i=1}^{N} s_i^2 + \sum_{i=1}^{N} \sum_{j=1, j\neq i}^{N} s_i s_j \tag{6}$$

However, the quantity $s_i s_j$ for a pair $i, j, i \neq j$ is

$$s_i s_j = \begin{cases} -l^2 \text{ with probability } 1/2 \\ +l^2 \text{ with probability } 1/2 \end{cases}, \tag{7}$$

so on average it will be zero. On the other hand s_i^2 will always be l^2, therefore

$$E[x^2(N)] = l^2 N. \tag{8}$$

after N steps. Since the average of x is zero, this is also the variance. We see that it increases linearly with time.

2.2 Relation to diffusion

We now see how random walks behave as the timestep τ tends to zero [16]. Let $P(i, N)$ denote the probability that a walker is at position i after N timesteps. Due to the equal probability for a walker to move left or right, we have the recursive equation:

$$P(i, N) = \frac{1}{2} P(i+1, N-1) + \frac{1}{2} P(i-1, N-1) \tag{9}$$

We write $x = il$ and $t = \tau N$, since these probabilities are scale-independent we find

$$P(x, \tau) = \frac{1}{2} P(x+l, t-\tau) + \frac{1}{2} P(x-l, t-\tau) \tag{10}$$

Subtracting $P(x, t-\tau)$ and dividing by τ, we have

$$\frac{P(x,t) - P(x,t-\tau)}{\tau} = \frac{l^2}{2\tau} \frac{P(x+l,t-\tau) + P(x-l,t-\tau) - 2P(x,t-\tau)}{l^2} \tag{11}$$

The left-hand side is a first order finite difference approximation of $\frac{\partial P}{\partial t}$ and the right-hand side is a first order approximation of $\frac{\partial^2 P}{\partial x^2}$. As τ and l tend to zero but $l^2/2\tau$ remains constant, we have

$$\frac{\partial P}{\partial t} = \frac{l^2}{2\tau} \frac{\partial^2 P}{\partial x^2}, \tag{12}$$

which is the well-known one-dimensional diffusion equation, a continuous process. A similar derivation can be achieved in arbitrary dimension.

3 Processing of Brownian motion sequences

In this section, we describe our sequence processing pipeline. The data we wish to process comes from a bespoke microfluidic device produced at ESIEE Paris [17]. The objective of this device is to allow the study of optical trapping at the micro scale. Because of the small size of the device and of the particles, existing particle tracking system do not work sufficiently well [18].

Pre-processing The sequences were recorded under a Leica inverted optical microscope, observing a capillary tube embedded in an optical trapping device. The tube contains the particles and is surrounded by the microfluidic system itself. Only the area containing the particles is of interest to us, so we first cropped the sequences around the capillary and automatically corrected the luminosity variations that occur during acquisition, by reference to the average image over the entire sequence. We then removed the non-moving components (fluidics system, capillary) by subtracting this average image. We named this pre-processed sequence $\mathcal{S}_0$. A sample frame from this output is shown on Fig. 1.

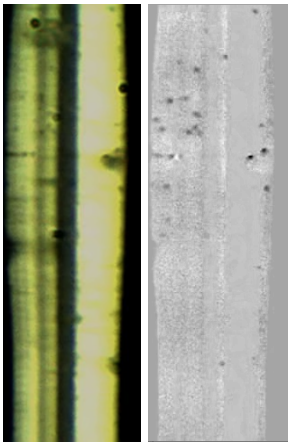

(a) (b)

Fig. 1. A sample frame from the initial sequence, and the output of the pre-processing for that frame.

Particle segmentation We simplified $\mathcal{S}_0$ using an area black top-hat on the h-maxima on each frame of the sequence:

$$\forall I \in \mathcal{S}_0, \quad I_{\text{hm}} = \varphi_R(I - h, I) - I \tag{13}$$

$$I_{\text{bta}} = I_{\text{hm}} - \gamma_\alpha(I_{\text{hm}}) \tag{14}$$

These are classical mathematical morphology operators [19]. φ_R is the closing by reconstruction [20]; γ_α is the area opening of parameter α [21], and h is the height parameter. These are efficiently implemented using the component tree [22,23].

This pipeline retains the particles and erases the background. It depends on few parameters. The area parameter α is twice the known area of the particles and h was hand-tuned at 15. We then smoothed the result using a 2D+t median filter on this sequence considered as a 3D image, of size $3\times3\times10$. We thresholded and denoised this sequence by erasing the very small remaining components via a small 3×3 opening. The result is named $\mathcal{S}_1^{3D}$.

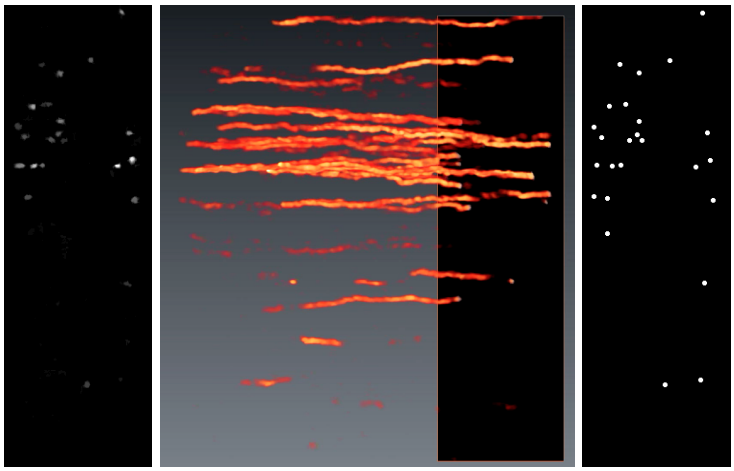

(a) (b) (c)

Fig. 2. In (a) the result of the black top-hat. In (b) the 2D+t traces. In (c), the segmented particles.

Trajectory separation We used a morphological erosion from a Euclidean distance map on $\mathcal{S}_1^{3D}$ to filter out small components and separate some traces. From this result, we estimated a discrete trajectory from the thresholded center on each slice. We then dilated these detected centroids with a disk in order to obtain a smooth and regular mask of the trajectories. We then computed the 3D skeleton of this binary mask [24]. Because the particles float in a 3D medium, they can appear to overlap and so their trajectory can merge. We detect crossing points in our skeleton that would cause non-unique labels on each slice. We then removed the triple points before labeling the trajectory.

Now that our trajectories are unique and identified, we dilated them with a disk with a greater radius than that of the particles to obtain a labeled mask.

Because the particles are round, a more precise way to find their centroids is to compute a weighted average of the coordinates of the pixels belonging to the trajectory in the mask according to the grey-level intensities of the initial sequence. We hence obtain sub-pixel accurate coordinates of the particles on each frame associated with a unique label ensuring the unicity of the tracking. We now study how to use these detected trajectories.

4 Particle tracking

We now wish to exploit the potential of Brownian motion for physical measurements

In (12), the quantity $l^2/2\tau$ is called the diffusion coefficient D.

$$D \equiv \frac{l^2}{2\tau} \tag{15}$$

Einstein [2] has shown that in a purely viscous fluid, with no external force influence

$$D \propto \frac{T}{\eta}, \tag{16}$$

where T is the absolute temperature and η the viscosity. In general these physical quantities are difficult to measure at the microscopic level. The study of diffusion via Brownian motion analysis is a potentially powerful method.

For this we assume neutrally buoyant, non-interacting test particles floating in a fluid and observed under a microscope. We assume that we are able to measure the position of these particles with arbitrary spatial and time resolution. This is not an outrageous demand, since Brownian motion is scale-independent, as we have seen. It means that we can trade some spatial and time resolution with each other.

4.1 Simulations

To assess the potential of Brownian motion to measure physical quantities, we simulate a 2D field with temperature varying in space and time, but with constant viscosity, where test particles are present.

Each particle is assumed to evolve independently of each other (no shocks or other interaction) irrespective of the density. To simulate temperature change, we vary the diffusion parameter D of equation (12) subject to arbitrary, but controlled change. This changes the expected spatial step according to (15). To measure the temperature, we allow ourselves to only use the parameters of the Brownian motion of each particle.

4.2 Mean square displacement

Because a single spatial step of an arbitrary particle can only be expected to resemble a random deviate from a Normal distribution of variance proportional

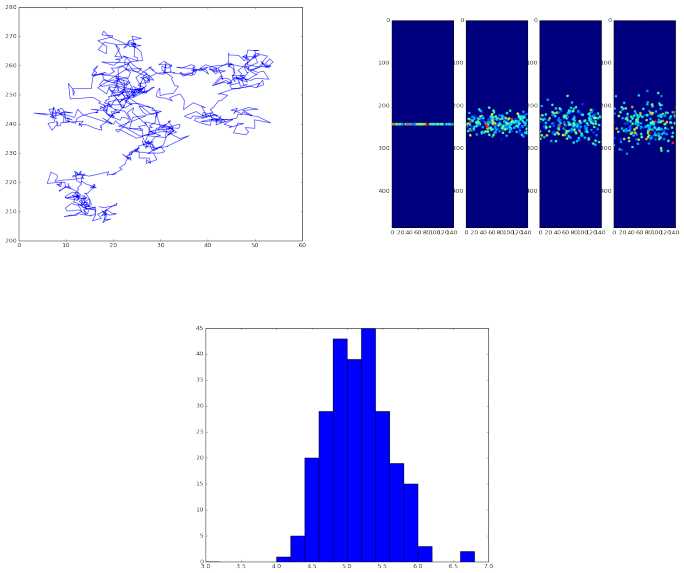

Fig. 3. . (a) A simulated random walk. (b) A simulation of a diffusive process by random walk at time 0, 50, 150 and 300 The color of each particle represents the estimation of the diffusion coefficient. (c) The dispersion of the diffusion coefficient estimation at time 100 over all particles.

to l^2, it cannot be used in isolation. Instead, we can estimate D by an averaging process. For this we define the mean square displacement (MSD) as follows:

$$\mathrm{MSD}(\tau) = E[\Delta \boldsymbol{r}^2(\tau)] = \frac{1}{m}\sum_{t=1}^{m} |\boldsymbol{r}(t+\tau) - \boldsymbol{r}(t)|^2, \tag{17}$$

where $\boldsymbol{r}(t)$ is the measured position of the studied particle at time t, and τ the timestep. Since $\mathrm{MSD}(\tau) = l^2/2n$, from (15), we should expect $\mathrm{MSD}(\tau)/2\tau$ to be constant and a reasonable approximation of D. To provide a stable estimate of the diffusion coefficient from a particle, we must consider a varying τ. In the discrete case, we can consider averaging the sequence $\mathrm{MSD}(n\tau)/n\tau$.

$$D \approx \frac{1}{2n}\sum_{i=1}^{n} \frac{\mathrm{MSD}(n\tau)}{n\tau}. \tag{18}$$

Averaging over several particles provides an even stabler estimation. On Fig 3, we show the output of a simulation of diffusing particles starting from a single line over time with a constant D. The color of each particle represents the estimate of the diffusion coefficient given by the motion analysis of that particle. For this estimation, we used $m = 150$ in (17) and $n = 5$ in (18). As seen in Fig. 3, the

estimation of this coefficient has a large variance but is still be usable. Indeed the simulated D was 5.0 and the median estimated D was 5.05.

4.3 Time-dependent analysis

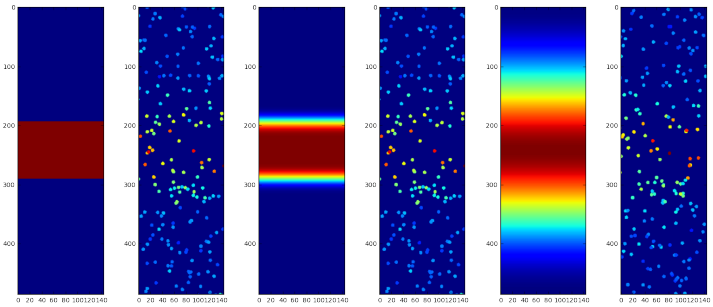

(a) t=0 (b) t=0 (c) t=100 (d) t=100 (e) t=200 (f) t=200

Fig. 4. Simulation of a cooling medium (a,c,e) sampled by the random walk analysis of 200 particles (b,d,f). Color code indicates the temperature, proportional to the local diffusion coefficient.

To test whether motion-derived estimates of the diffusion coefficient are sufficiently precise, we simulate a time-dependent process illustrated on Fig. 4. In this test, a hot rectangular area is allowed to cool over time by conduction in a cooler medium. 200 particles are uniformly randomly placed and tracked over time. The estimated MSD is computed and associated with each particle and is color-coded with the same scheme. Since the problem is really only 1D+t, as there is no variation along the horizontal x axis, we can project all the estimated MSD onto the vertical y axis, as shown on Fig. 5(a). The MSD estimation is quite sparse, so it is beneficial to interpolate it. To achieve this, we used 2D universal kriging [25,26]. Our input data are all the traces points with their estimated diffusion coefficients.

In this experiment, D is estimated over 150 causal trace steps, so to avoid border effects, the last 150 steps are not estimated, shortening the sequence by that amount. As we can see in Fig. 5(c), the estimation is now of reasonable quality and appears bias-free.

5 Results on real data

Starting from our estimated traces from section 3, we first verify their random walk qualities, then estimate the diffusion coefficient image in the same way as in the simulation.

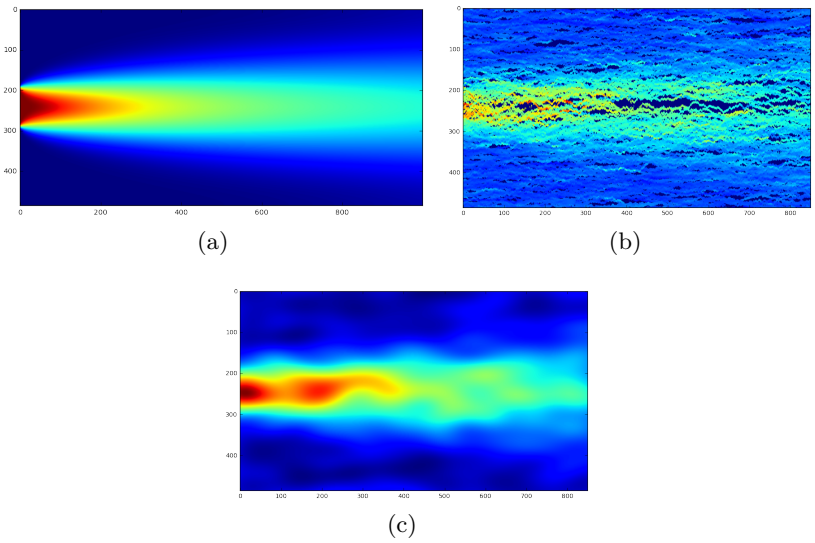

Fig. 5. (a): 1D+t ground-truth representation of the diffusion coefficient in the cooling medium of Fig 4.(b): Superposition of the trace estimation for the diffusion coefficient D. (c) 2D Kriging estimation of the same diffusion coefficient. The color code is the same in all three images.

On Fig. 6, we show the trace of one of the particle over time, and we estimate the associated MSD from (17). We note the subpixel accuracy of the trace, and the linear aspect of MSD(τ) with respect to τ. All sufficiently long trace (time length > 150 step) were found to exhibit similar characteristics. From these we estimate the MSD at every point of all the segmented traces, and interpolated the data as above. This is illustrated on Fig. 7.

On this experiment, the particles were held in an optical trap before $t = 0$ and then released at that time. We expect the particles to diffuse and heat as they move into the medium, i.e. we expect the traces to expand and become redder in the false-color rendition of the result, which is what we are indeed observing.

6 Conclusion

In this article we have shown that subpixel-accurate trace analysis of the Brownian motion of microscopic particles is possible, even in challenging situations, and that it can provide estimates of the local diffusion coefficient, which is proportional to the temperature divided by the viscosity of the medium. We have provided a full pipeline, validated on simulated data and tested on real data. Future work will validate the physical measurements in more controlled acquisitions where a stable temperature gradient can be established. Also, the current

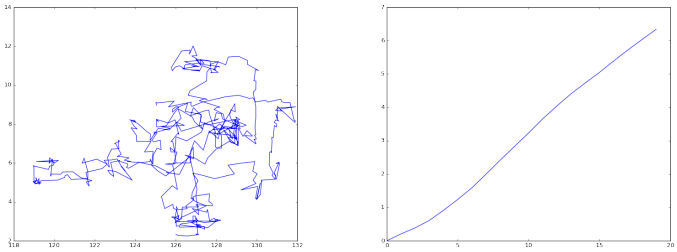

(a) (b)

Fig. 6. (a) The trace of a real particle. Note the subpixel accuracy of the trace and similarity to Fig. 3(a) ; (b) the MSD(τ) vs. τ associated with this trace, which is linear as expected.

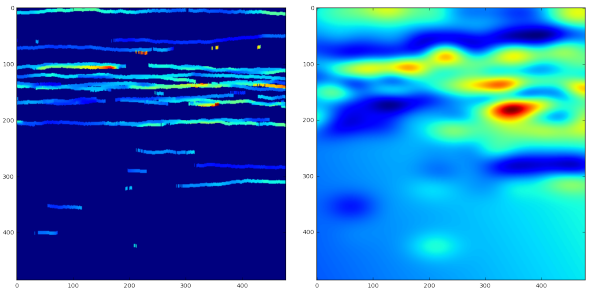

Fig. 7. (a) Real, segmented traces with associated estimated MSD as in Fig. 5. (b) Interpolated MSD.

diffusion coefficient estimation includes an integrating step over a long period (150 time steps in our study) for accuracy. This integration blurs the estimation in time and in the direction of the particle travel. We plan to correct this effect by considering it as an inverse problem.

References

1. Brown, R.: A brief account of microscopical observations made in the months of june, july and august, 1827, on the particles contained in the pollen of plants; and on the general existence of active molecules in organic and inorganic bodies. Phil. Mag. **4** (1828) 161–173
2. Einstein, A.: Über die von der molekularkinetischen theorie der wärme geforderte bewegung von in ruhenden flüssigkeiten suspendierten teilchen. Annalen der Physik **322**(8) (1905) 549–560
3. Perrin, J.: Mouvement brownien et réalité moléculaire. Ann. Chim. Phys., **18**(8) (1909) 5–114

4. Bachelier, L.: Théorie de la spéculation. Annales Scientifiques de l'École Normale Supérieure **3**(17) (1900) 21–86
5. Skellam, J.G.: Random dispersal in theoretical populations. Biometrika **38**(1/2) (1951)
6. Colding, E., et al.: Random walk models in biology. Journal of the Royal Society Interface (2008)
7. De Gennes, P.G.: Scaling Concepts in Polymer Physics. Cornell University Press, Ithaca and London (1979)
8. Grady, L.: Random walks for image segmentation. IEEE T. Pattern Anal. Mach. Intell. **28**(11) (2006) 1768–1783
9. Metropolis, N., Rosenbluth, A.W., Rosenbluth, M.N., Teller, A.H., Teller, E.: Equation of state calculations by fast computing machines. The journal of chemical physics **21**(6) (1953) 1087–1092
10. Hastings, W.: Monte carlo sampling methods using markov chains and their applications. Biometrika **57**(1) (1970) 97–109
11. Geman, S., Geman, D.: Stochastic relaxation, gibbs distributions, and the bayesian restoration of images. IEEE T. Pattern Anal. Mach. Intell. **6** (1984) 721–741
12. Bertsimas, D., Vempala, S.: Solving convex programs by random walks. Journal of the ACM (JACM) **51**(4) (2004) 540–556
13. Park, J., Choi, C., Kihm, K.: Temperature measurement for a nanoparticle suspension by detecting the brownian motion using optical serial sectioning microscopy (ossm). Measurement Science and Technology **16**(7) (2005) 1418
14. Donsker, M.: An invariance principle for certain probability limit theorems. Memoirs of the American Mathematical Society **6** (1951)
15. Pólya, G.: Über eine aufgabe betreffend die irrfahrt im strassennetz. Math. Ann. **84** (1921) 149–160
16. Nordlund, K.: Basics of monte carlo simulations
17. Gaber, N., Malak, M., Marty, F., Angelescu, D.E., Richalot, E., Bourouina, T.: Optical trapping and binding of particles in an optofluidic stable fabry–pérot resonator with single-sided injection. Lab on a chip **14**(13) (2014) 2259–2265
18. Allan, D., et al.: Trackpy: Fast, flexible particle-tracking toolkit
19. Najman, L., Talbot, H., eds.: Mathematical Morphology: from theory to applications. ISTE-Wiley, London, UK (September 2010) ISBN 978-1848212152.
20. Vincent, L.: Morphological grayscale reconstruction in image analysis: Applications and efficient algorithms. Image Processing, IEEE Transactions on **2**(2) (1993) 176–201
21. Vincent, L.: Grayscale area openings and closings, their efficient implementation and applications. In: Proceedings of the conference on mathematical morphology and its applications to signal processing, Barcelona, Spain (May 1993) 22–27
22. Meijster, A., Wilkinson, H.: A comparison of algorithms for connected set openings and closings. IEEE T. Pattern Anal. Mach. Intell. **24**(4) (April 2002) 484–494
23. Géraud, T., Talbot, H., Vandroogenbroeck, M.: Algorithms for mathematical morphology. [19] chapter 12 323–354 ISBN 978-1848212152.
24. Bertrand, G., Couprie, M.: Transformations topologiques discretes. In Coeurjolly, D., Montanvert, A., Chassery, J., eds.: Géométrie discrète et images numériques. Hermès (2007) 187–209
25. Matheron, G.: The theory of regionalized variables and its applications. Volume 5. École national supérieure des mines (1971)
26. Olea, R.A.: Optimal contour mapping using universal kriging. Journal of Geophysical Research **79**(5) (1974) 695–702